ADVANCED MATERIALS TECHNOLOGIES
www.advmattechnol.de

Toward the Potential Scale-Up of $Sn_{0.9}Mn_{0.1}O_2||LiNi_{0.6}Mn_{0.2}Co_{0.2}O_2$ Li-Ion Batteries – Powering a Remote-Controlled Vehicle and Life Cycle Assessment

Adele Birrozzi, Sebastián Pinto Bautista, Jakob Asenbauer, Tobias Eisenmann, Thomas E. Ashton, Alexandra R. Groves, Chris Starkey, Jawwad A. Darr, Dorin Geiger, Ute Kaiser, Guk-Tae Kim, Marcel Weil, and Dominic Bresser**

Academic research in the battery field frequently remains limited to small coin or pouch cells, especially for new materials that are still rather far from commercialization, which renders a meaningful evaluation at an early stage of development challenging. Here, the realization of large lab-scale pouch cells comprising $Sn_{0.9}Mn_{0.1}O_2$ (SMO), prepared via an easily scalable hydrothermal synthesis method, as an alternative active material for the negative electrode and $LiNi_{0.6}Mn_{0.2}Co_{0.2}O_2$ (NMC_{622}) as a commercially available active material for the positive electrode is reported. Nine double-layer pouch cells are connected in series and parallel, suitable for powering a remote-controlled vehicle. Subsequently, these SMO||NMC_{622} cells are critically evaluated by means of an early-stage life cycle assessment and compared to graphite||NMC_{622} cells, in order to get first insights into the potential advantages and challenges of such lithium-ion chemistry.

1. Introduction

About 30 years after their first introduction on the market, lithium-ion batteries (LIBs) are the dominating battery technology to power portable electronic devices and (hybrid) electric vehicles, while they are also playing an increasingly important role for stationary energy storage applications.[1–5] Not least owing to this tremendous success, the Nobel Prize in Chemistry 2019 was awarded to some of the scientists that have contributed in a truly outstanding manner to this development.[6,7] It is important to note, however, that the term 'lithium-ion battery' does not specify a certain battery chemistry, i.e., neither the active material for the negative and positive electrode, nor the electrolyte composition or other cell components. Especially with regard to the positive electrode, several materials have been commercialized, including $LiCoO_2$ (LCO, the very first active material for the positive electrode in LIBs),[8] $LiNi_{1-x-y}Mn_xCo_yO_2$ (NMC), $LiNi_{0.8}Co_{0.15}Al_{0.05}O_2$ (NCA), as well as $LiFePO_4$ (LFP), while others such as $LiNi_{0.5}Mn_{1.5}O_4$ (LNMO) have reached a rather mature development stage already.[1,2] For the negative electrode, though, the choice of commercial active materials is essentially limited to (natural or synthetic) graphite – potentially with a minor fraction of Si or SiO_x, and in a few cases also $Li_4Ti_5O_{12}$ as high-power, long lifetime alternative (but at the expense of a substantially lower energy density).[2,9] An alternative commercialized active material that has provided a superior energy density, is a composite of tin, cobalt, and carbon.[10] Nevertheless, this anode chemistry was ultimately commercially unviable due to the lack of availability and high cost of cobalt, the challenging synthesis, and the rather short cycle life of cells.[11–14] At the same time, further optimization of graphite-based negative electrodes appears very limited, motivating the search for alternatives that provide enhanced energy and power density, while simultaneously ensuring safe operation of the battery cell.[3,15–18] A rather recently proposed class of

A. Birrozzi, S. P. Bautista, J. Asenbauer, T. Eisenmann, G.-T. Kim, M. Weil, D. Bresser
Helmholtz Institute Ulm (HIU)
89081 Ulm, Germany

A. Birrozzi, J. Asenbauer, T. Eisenmann, G.-T. Kim, D. Bresser
Karlsruhe Institute of Technology (KIT)
76021 Karlsruhe, Germany
E-mail: dominic.bresser@kit.edu

The ORCID identification number(s) for the author(s) of this article can be found under https://doi.org/10.1002/admt.202200353.

DOI: 10.1002/admt.202200353

S. P. Bautista, M. Weil
Institute for Technology Assessment and Systems Analysis (ITAS)
Karlsruhe Institute of Technology (KIT)
76021 Karlsruhe, Germany
E-mail: marcel.weil@kit.edu

T. E. Ashton, A. R. Groves, C. Starkey, J. A. Darr
University College London (UCL)
Department of Chemistry
London WC1H 0AJ, United Kingdom

D. Geiger, U. Kaiser
Central Facility for Electron Microscopy
Ulm University
89081 Ulm, Germany

active materials that is combining the "classic" alloying and conversion reaction with lithium are conversion-alloying materials (CAMs).[19] These materials are commonly based on the oxide or sulfide of an alloying element such as zinc, germanium, or tin, which have been intensively studied in different compositions and morphologies due to their high capacities and low working voltage,[13,20,21] and contain additionally a small amount of one or more transition metals that confines the aggregation of the alloying element and ensures a sufficient electronic conductivity within the initial primary particles to enable the reversible formation of Li_2O.[19,22–35] As already shown in a previous study, the incorporation of the Mn dopant into the SnO_2 structure allows for stable cycling and high reversible capacities with good rate performance, precisely, 1276 mAh g^{-1} at 20 mA g^{-1} and 651 mAh g^{-1} at 2 A g^{-1}, for instance.[34] A first estimation of the achievable specific energy revealed a potential improvement, e.g., for LIBs comprising $Sn_{0.9}Mn_{0.1}O_2$ (SMO) as the active material for the negative electrode and LNMO for the positive electrode with about 480 Wh kg^{-1} compared to 454 Wh kg^{-1} for a LIB containing graphite and LNMO (based on the mass of the active materials only, experimental data for the anode and theoretical data for the cathode).[34] These findings were corroborated by a subsequent lab-scale study on (nonoptimized) full-cells employing a cobalt and manganese-containing tin oxide anode and an LNMO cathode, yielding 312 Wh kg^{-1} [32] compared to 259 Wh kg^{-1} that had been reported earlier for a comparable lab-scale graphite||LNMO full-cell.[36] Remarkably, more than 85% of the total capacity of the SMO||LNMO full-cell was provided at a cell voltage >3 V, allowing for the stable operation of electronic devices.[32] Nonetheless, all these studies were based on rather small electrodes with a diameter of slightly more than 1.1 cm^2 and the use of Swagelok-type T-cells, i.e., rather far still from any industrially relevant setup. Moreover, any potential use of new active materials should be ideally critically evaluated concerning the potential economic and environmental impact at an early stage of development.[37–43] The challenges for the required life cycle assessment (LCA), however, are greater for less mature technologies.

Herein, we report the scale-up of an $Sn_{0.9}Mn_{0.1}O_2$ (SMO) based lithium-ion cell, using $LiNi_{0.6}Mn_{0.2}Co_{0.2}O_2$ (NMC_{622}) as the active material for the positive electrode, owing to the commercial availability of the latter. Using these materials facilitated the subsequent LCA and comparison with a graphite analog, i.e., graphite||NMC_{622} cells, which are already largely used in everyday life. The resulting pouch-type cells were connected in parallel and in series to power an electric remote-controlled vehicle. As such studies on lab-scale prototyping and the critical evaluation of the potential environmental impact of new, noncommercial materials and cell chemistries are very rare in literature, we hope that this work will motivate also others to go one step beyond the common lab-scale studies and, thus, support the potential transfer of scientific research into commercial applications.

2. Results and Discussion

2.1. Development of a Lab-Scale Battery Pack to Power a Remote-Controlled Vehicle

In a first step, we compared the estimated specific energy of SMO||NMC_{622} lithium-ion cells and the graphite||NMC_{622} reference. The estimation of the specific energy at the active material level based on experimental values for the anodes and theoretical values for the cathodes, as described in the Experimental Section, yields a specific energy of 456 Wh kg^{-1} for the reference cell and a slightly higher specific energy of 468 Wh kg^{-1} for the SMO||NMC_{622} cell (see also Table S1, Supporting Information). It should be noted that this estimation (in both cases) did not include the first cycle irreversibility, which is an issue that still needs to be addressed for SMO-type anodes – for instance, by advances concerning the material design[44,45] and the development of suitable pre-lithiation strategies.[46,47] For the estimation of the specific energy at the cell level, the BatPaC tool developed by the Argonne National Laboratory in the USA, was used, suggesting an energy density of 231 Wh kg^{-1} for the graphite||NMC_{622} reference cell, i.e., approximately half of the specific energy at the active material level. Assuming a comparable overall cell composition, the same ratio was used for the estimation of the specific energy of the SMO||NMC_{622} at the cell level, yielding 237 Wh kg^{-1}. Considering the good rate capability of tin oxide-based anodes,[32,34] and the potential, relatively greater increase in energy density when rising the upper cut-off voltage of such full-cells,[48,49] these values are generally promising, which motivated us to go ahead with the exemplary scale-up of such lithium-ion cells.

Figure 1. Photograph of the remote-controlled vehicle with the commercial battery pack.

For this purpose, we selected a suitable electronic device to be powered by our self-designed battery pack, a device that is sufficiently large and to which our battery cells can be rather easily connected. We finally chose a remote-controlled electric vehicle (**Figure 1**).

According to the product specifications the vehicle requires a battery pack with an overall voltage of 9 V. We thus recorded the charge and discharge voltage of a small-scale SMO||NMC_{622} lithium-ion cell (**Figure 2**a) in order to estimate how many cells we needed to connect in series to reach at least 9 V. Given the average full-cell voltage of about 3.0 V upon discharge (as indicated by the orange arrows in Figure 2a), we opted for three cells in series. For the design of the battery pack, however, we also needed an idea of the required current that was not mentioned in the product specifications. Therefore, we connected the remote-controlled vehicle without any battery to a potentiostat, set the voltage to 9 V, and started to

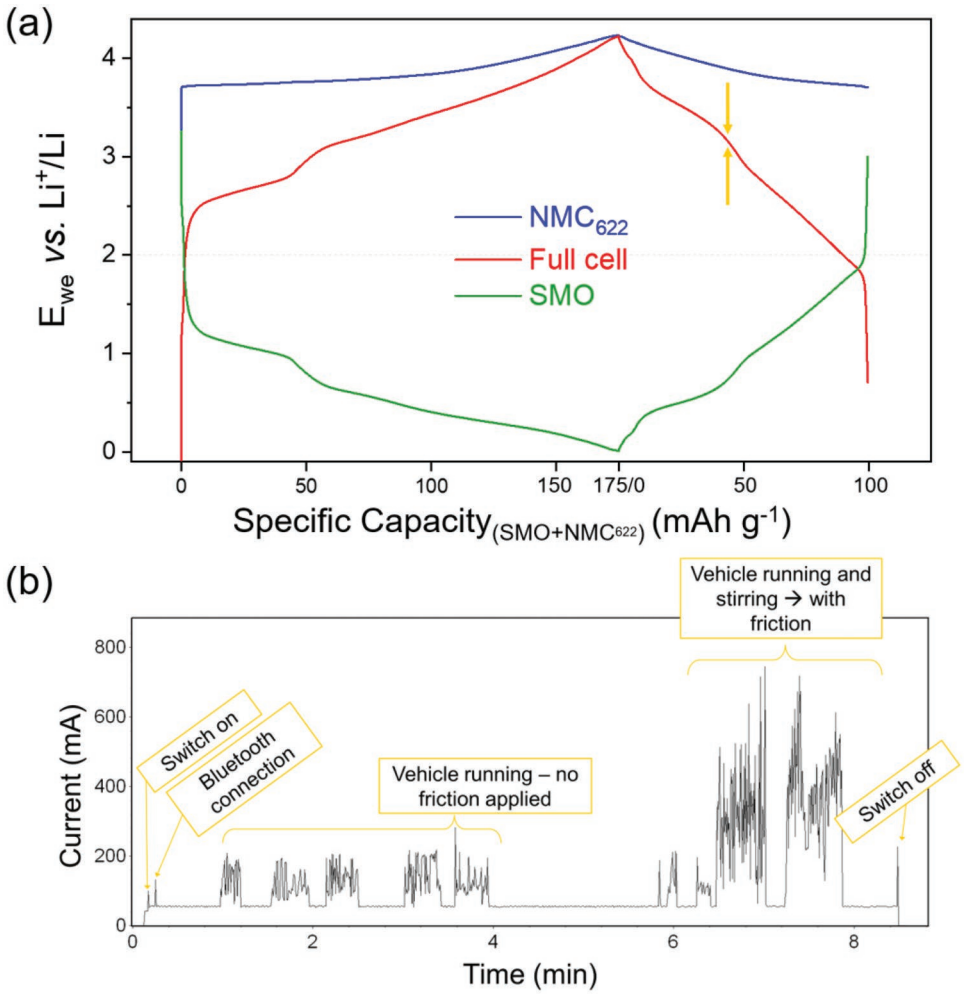

Figure 2. a) Exemplary charge and discharge profile of a SMO||NMC_{622} cell (in red), cycled in a three-electrode configuration in order to deconvolute the contribution of the anode (in green) and cathode (in blue); the orange arrows are indicating the average discharge voltage of the full-cell. b) Utilization profile of the remote-controlled vehicle, showing the current recorded when setting the voltage to 9.0 V; the different typical "current events" are indicated in the profile.

"drive" the vehicle (upside down in order to stay connected with the potentiostat) while recording the current. To simulate the friction of the floor during driving, we applied a homogeneous pressure on the tires. Figure 2b shows the resulting utilization profile with an indication of the different "current events". This experiment showed that the vehicle required an average current of 350 mA.

Considering a meaningful operation time of the battery pack, we chose a double-side coated NMC_{622} cathode with an areal capacity of 3.5 mAh cm^{-2} and punched squared electrodes of 4×4 cm^2, resulting in a total capacity of 112 mAh. With three cells connected in parallel, this would provide a total capacity of 336 mAh, so sufficient to power the remote-controlled electric vehicle for about one hour. The SMO anode was designed accordingly with a slight capacity excess in the first charge to avoid any potential lithium plating. As the average first discharge capacity was found to be about 1600 mAh g^{-1}, we prepared electrodes with an average active material mass loading in the range from 2.5 to 3.0 mg cm^{-2}, resulting in an areal capacity of 4.0–4.8 mAh cm^{-2}, i.e., slightly larger than the areal capacity of the NMC_{622} cathode. To ensure a good alignment of the two electrodes, the anode was cut with somewhat larger dimensions of 4.4×4.4 cm^2.

The resulting pouch cells (see Figure S1, Supporting Information for a schematic illustration of the single cells) were connected in series and parallel as depicted in **Figure 3**a,b. The open-circuit voltage in the charged state was 11.4 V, i.e., sufficiently high for powering the remote-controlled vehicle and the total capacity was about 336 mAh. The eventual battery pack was connected to the vehicle as displayed in Figure 3c and the successful use of the developed battery pack is presented in Video S1, Supporting Information. The car was running for >3 h and is still running. It is interesting to note that the complete lithium-ion battery pack had a total volume of around 60 cm^3 with a weight of 62 g. Both the volume and the mass were substantially lower than the commercial alkaline battery pack that is commonly used for such remote-controlled vehicles with about 100 cm^3 and 165 g, respectively. This improvement is generally expected with regard to the common energy density of the different battery technologies,[50] but still nicely highlights

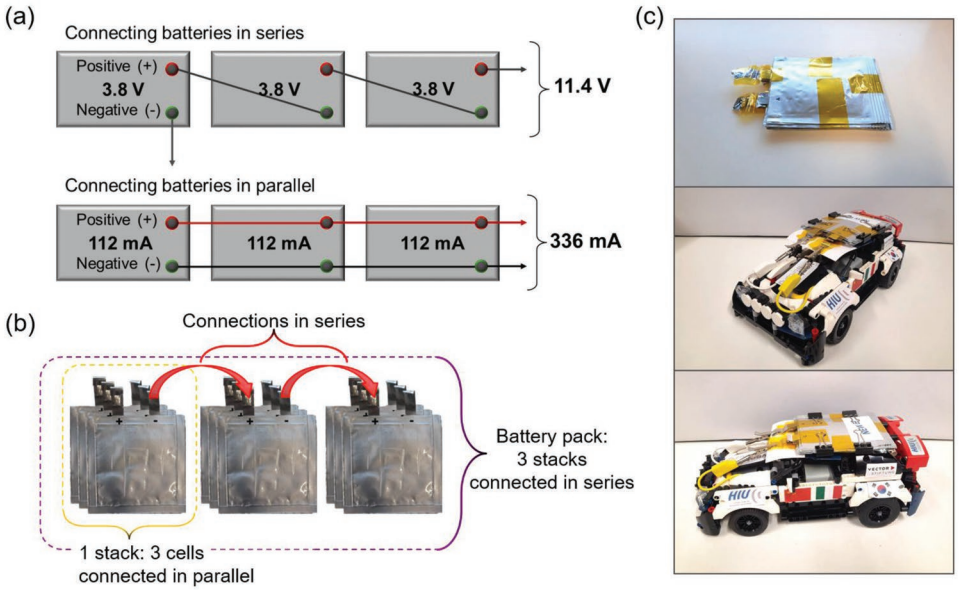

Figure 3. Schematic illustration of the battery pack design with a) the impact of connecting three pouch cells in series and parallel and b) photographs of the assembled pouch cells to power the remote-controlled vehicle. c) Photographs of the battery pack and the battery pack connected to the remote-controlled vehicle.

the general advantages of (secondary) lithium-ion batteries over (primary) alkaline batteries.

2.2. Life Cycle Assessment – The SMO Active Material

Following these intriguing results, we conducted a critical LCA of this alternative battery cell chemistry. Given the early stage of development, this "preliminary" or "prospective" LCA certainly just serves as a starting point and will have to be conducted again at a later stage, but such "development-accompanying" analysis helps to identify particularly critical aspects that might thus be addressed at a rather early stage to ensure compliance with sustainability criteria.

In a first step, a basic evaluation of the SMO synthesis was performed, yielding the expected phase-pure rod-like SMO particles (Figure S2, Supporting Information).[32,51] The continuous hydrothermal flow method was chosen because of the potential scale-up and the proven suitability for yielding high-performance transition metal-doped SnO_2 for application as the active material in lithium-ion anodes.[32,51] The synthesis procedure is briefly summarized in **Figure 4**. In brief, the precursor solutions are pumped together into a T-piece mixer at room temperature to obtain a homogeneous solution. Simultaneously, deionized water is heated to 450 °C at a pressure of 24.1 MPa to form supercritical water, which is then pumped into a confined jet mixer. Therein, it is combined with the precursor solutions and a turbulent mixing develops, resulting

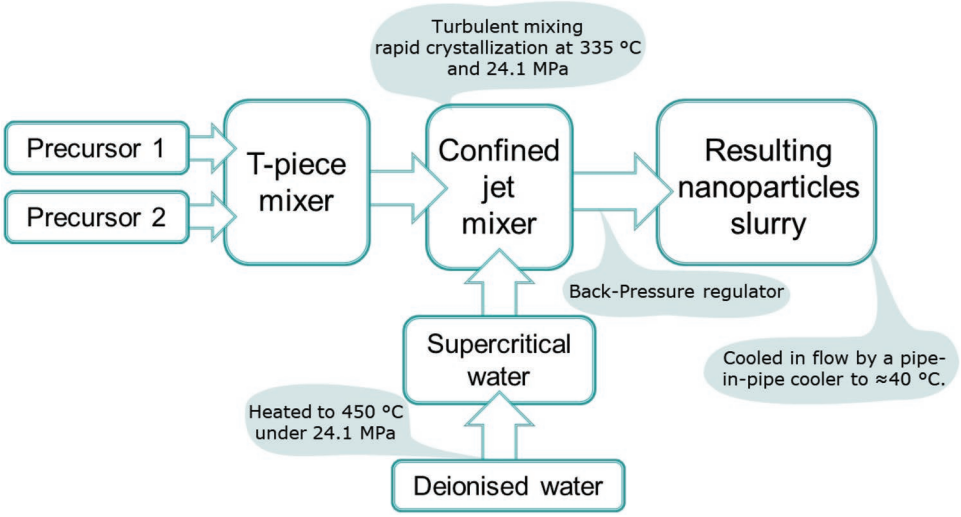

Figure 4. Simplified illustration of the continuous hydrothermal flow synthesis apparatus to produce the SMO active material.

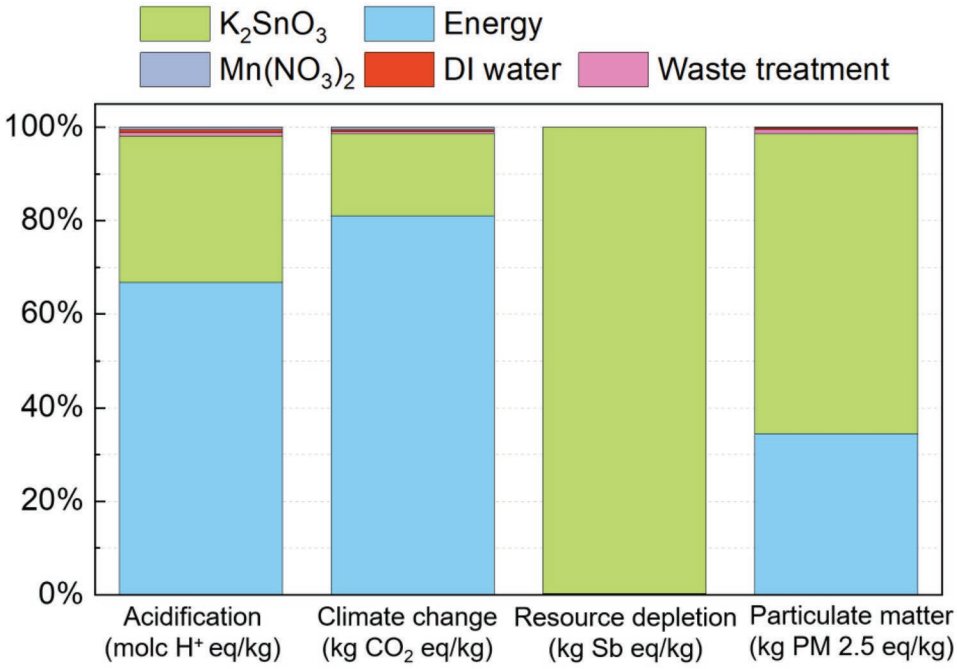

Figure 5. Life cycle impact per kg of SMO that is synthesized, divided into the four categories "acidification", "climate change", "resource depletion", and "particulate matter" with an indication of the relative contribution of the two precursors K_2SnO_3 and $Mn(NO_3)_2$, the waste treatment, and the consumption of deionized (DI) water.

in a rapid crystallization of nanoparticles. Subsequently, the aqueous slurry containing the nanoparticles is cooled down to about 40 °C and led through a back-pressure regulator. Finally, the slurry is washed several times with deionized water via dialysis and, eventually, freeze-dried to yield a fine SMO powder.

In **Figure 5**, the total life cycle impact per kg of SMO active material produced is presented, divided into the four categories "acidification", "climate change", "resource depletion", and "particulate matter". For each category, the relative impact of selected synthesis parameters is indicated, including the energy demand, the two precursors K_2SnO_3 and $Mn(NO_3)_2$, the waste treatment, and the consumption of deionized (DI) water. There are essentially two main contributors that have an environmental impact: the energy demand and the precursor K_2SnO_3. The energy demand includes the electricity used for the operation of the pumps and drying ovens and dominates the impact categories "acidification" and "climate change". Additionally, it significantly contributes to the "particulate matter" potential. The impact is pronounced owing to the use of energy from the average European electricity mix, which is characterized by a significant contribution from the combustion of fossil fuels, leading to the release of greenhouse gases, sulfur dioxide, and particulates into the atmosphere. The synthesis of SMO currently requires the use of two pumps to deliver the different precursors and one pump to deliver the DI water; the latter pump flow is connected to a heater to generate supercritical water inflow and is contributing with almost 40% to the total energy demand, while the contribution of the remaining pumps is negligible. The operation of the oven to dry the SMO slurry is the process with the largest specific energy demand, amounting to about 60%. Especially this process provides great potential for further improvement given the non-optimized nature of a pilot-scale production line. It can be inferred that scaling up the SMO synthesis might lead to a significant decrease in the energy needed for this step. The second large contribution is the potassium stannate precursor and its supply chain. It accounts for most of the total impact related to resource depletion. The extraction and refining of tin are considered to be of greatly polluting nature due to the release of large amounts of sulfur dioxide (SO_2) and other particulates, while the material itself is deemed as a critical resource.

In a second step, the same impact analysis was performed for the SMO/NMC_{622} anode/cathode chemistry by including the impact of the NMC_{622} cathode and the results were compared with the graphite/NMC_{622} reference cell chemistry. For this analysis, the earlier estimated specific energy of the different cell chemistries at the active material level and the anode/cathode ratio were taken into account in order to calculate the specific impact per unit of energy storage capacity. **Figure 6** illustrates the relative impacts of the anode and cathode for the two cell chemistries with regard to the four categories introduced along with Figure 5. For this comparison, an additional scenario for the SMO/NCM_{622} cell chemistry was included, referred to as 'optimistic' (i.e., $SMO_{baseline}$ and $SMO_{optimistic}$), which considered the potential improvements for the SMO synthesis in the case of the scale-up to an industrial level. In this 'optimistic' scenario, a product yield (Y) of 95% was used (in contrast to a 75% yield in the 'baseline' scenario) and the energy demand was reduced to half of the 'baseline' value, herein referred to as an energy use factor (EUF) of 0.5. Different strategies may be considered in order to achieve such increase in the yield: First, the synthesis parameters (time, temperature, pH, reagent concentration, pressure, reagent salts) have not been optimized, yet, which certainly provides room

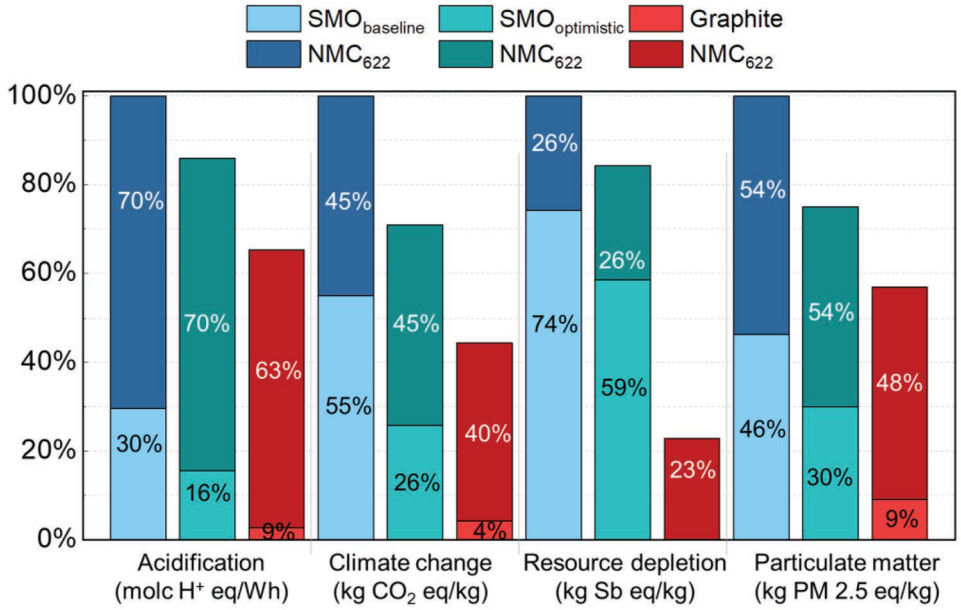

Figure 6. Relative life cycle impact per unit of energy storage capacity for the SMO/NMC_{622} cell chemistry – once with the current input data for the SMO synthesis ($SMO_{baseline}$) and once considering the scale-up of the synthesis going along with an enhanced yield and energy efficiency ($SMO_{optimistic}$) as specified in the text – and the graphite/NMC_{622} cell chemistry for comparison. All percentage values refer to the maximum impact obtained for one of these cell chemistries.

for improving the product yield. Second, when pumping the metals/base into the reactor, the reagents take a short amount of time to reach a stable concentration due to diffusion of the reagents in the pipes prior to meeting the mixing point. As such, the first and last milliliters of the product are discarded to ensure that the collected product is homogenous. At larger production scales, the amount of discarded material becomes insignificant compared to the amount collected, leading to a significant improvement of the yield. Furthermore, the process would certainly be streamlined, thus, removing any losses from manual handling. For instance, when the material is centrifuged/dialyzed/freeze-dried, there are inevitable losses. At scale, these would certainly be minimized. Additionally, other techniques such as heat recovery may lead to improved energy efficiency.

In almost all cases, the NMC_{622} cathode has a relatively larger impact for each category, which is not least related to the larger mass fraction due to the lower specific capacity of NMC_{622} compared to graphite and SMO. There is only one exception: the "resource depletion" in the case of SMO, which substantially exceeds the relative impact of NMC_{622}, as also tin (just like cobalt and lithium) is considered a critical resource. While the impact is significantly reduced in the optimistic scenario already, it should also be noted that this estimation of the life cycle impact does not take into account potential geopolitical constraints that might have an effect on the supply chain. Since this might be particularly relevant for cobalt,[52] the relative impact of NMC_{622} might be generally underestimated here. Also, the comparison SMO vs. graphite has to be taken with some care. The values for SMO were calculated based on the direct input from the synthesis, while the values for graphite were taken from the Ecoinvent database. In that case, very conservative assumptions of the power and energy demand were used in the model, while the production of battery-grade graphite and its related impacts generally entail a high degree of uncertainty, as reported by Ecoinvent, due to the noncomprehensive and little amount of data available, as also explicitly noted in the description of the respective dataset. In fact, according to a recent LCA study using primary data from a Chinese graphite manufacturer, the global warming potential (GWP) related to the production of battery-grade graphite is more than four times higher than the GWP found in the Ecoinvent database 3.7.1.[53] When taking the previous into consideration, it is likely that the difference in environmental performance between both chemistries will become narrower and more in favor of the SMO/NMC_{622} chemistry – initially, with regard to the GWP category and potentially also affecting the other categories.

In a third step, the complete SMO||NMC_{622} battery cell was evaluated to calculate the total footprint, which facilitates the comparison with other systems reported in the literature (see also Table S3, Supporting Information for the cell composition). Such calculation of the aggregated impacts at the cell level moreover serves to illustrate the relevance of the anode and each component in the overall footprint of the system. **Figure 7** displays the relative contributions with regard to the four impact categories. In general, the two electrodes have the greatest impact, accounting for more than half of the total impact in all four categories. The third greatest factor is the cell manufacturing owing to its high energy intensity, specifically the electricity needed for maintaining a suitably dry atmosphere for several stages of the cell assembly. The contribution of the other cell components appears rather negligible in comparison at this stage of the evaluation.

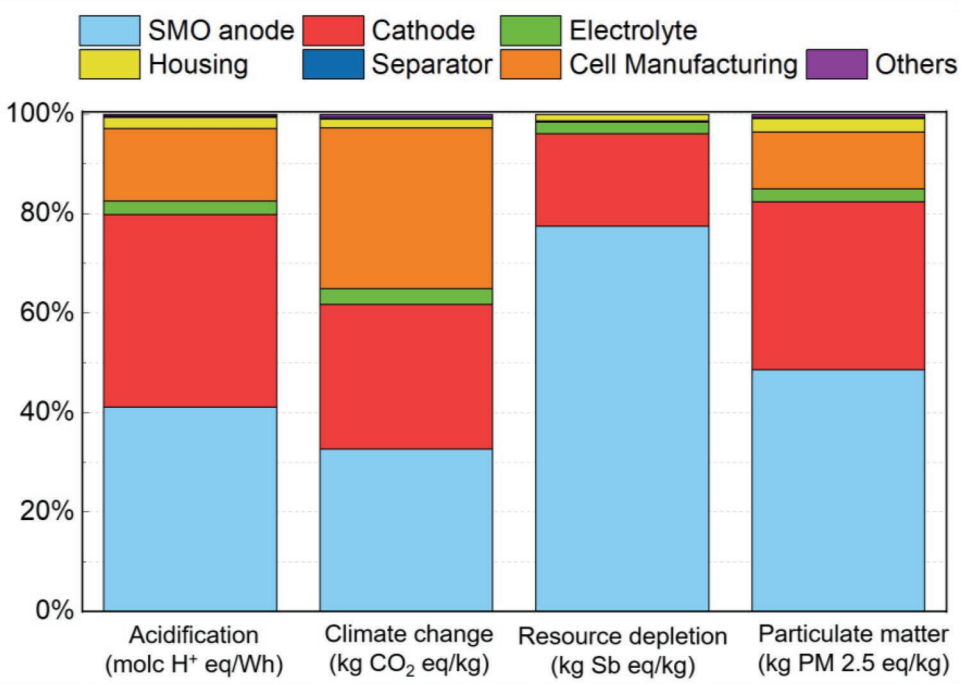

Figure 7. Comparative life cycle impact analysis of the different cell components for the SMO||NCM_{622} battery chemistry with regard to the four categories "acidification", "climate change", "resource depletion", and "particulate matter". Note that the impact of each category was normalized to 100%, while the absolute values differ quite substantially with 6.5×10^{-4}, 7.2×10^{-2}, 7.9×10^{-5}, and 6.1×10^{-5} for the four categories (see also Table S2, Supporting Information), respectively.

In the following, a more dynamic evaluation of the life cycle impact of the SMO synthesis is provided in the form of a sensitivity analysis, which also serves to assess the uncertainty when studying systems at an early development stage. As discussed above, the most critical impact factors are the energy demand – in other words, the energy use factor (EUF) – and the production yield (*Y*); these two factors had also been modified above for the 'optimistic' scenario. In **Figure 8**, the sensitivity of the total environmental impact of the cell as a function of a varying EUF for the SMO synthesis is depicted. The improvement of the EUF to 0.5 in the most favorable scenario would lead to a reduction of the 'cumulative energy demand' (CED) to about 90% and a similar drop of the 'climate change' potential. A little less affected are the 'acidification' and 'particulate matter' potentials, while negligible effects are observed for the "resource depletion". The latter, however, is the most sensitive toward changes in *Y* (**Figure 9**). Increasing this to the theoretical maximum, i.e., $Y = 100\%$, would result in a reduction of the impact of the 'resource depletion' to 86.9%. Nonetheless, also the other impact categories would be considerably affected by increasing *Y*, which is, in fact, rather straightforward, as any increase in *Y* results in a significant reduction of, for instance, the 'CED' or 'climate change' per mass unit of SMO.

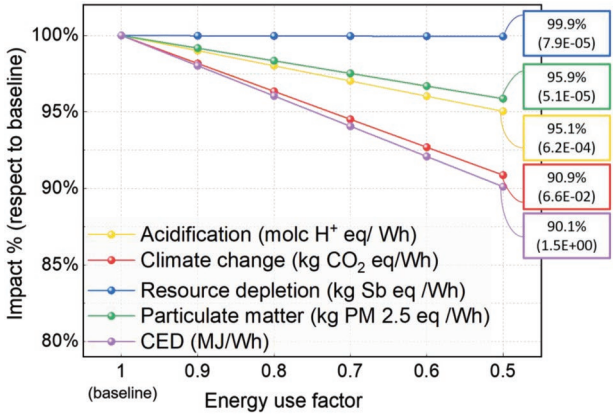

Figure 8. Sensitivity of the environmental impact categories "acidification", "climate change", "resource depletion", and "particulate matter" on a variation of the energy use factor (EUF) for the SMO synthesis.

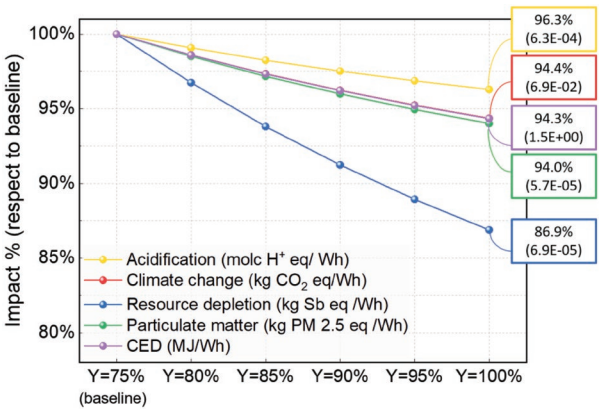

Figure 9. Sensitivity of the environmental impact categories "acidification", "climate change", "resource depletion", and "particulate matter" on a variation of the production yield (*Y*) for the SMO synthesis.

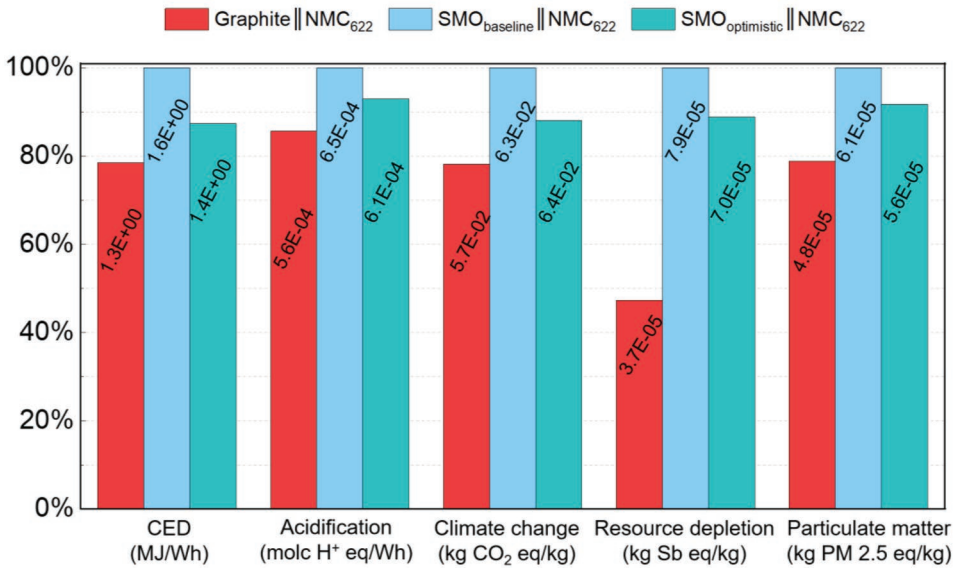

Figure 10. Comparison of the environmental footprint with regard to the "CED", "acidification", "climate change", "resource depletion", and "particulate matter" for the $SMO_{baseline}||NMC_{622}$, the $SMO_{optimistic}||NMC_{622}$, and the graphite$||NMC_{622}$ cell. The total values are indicated in the corresponding columns (see also Table S2, Supporting Information) and the maximum of 100% always corresponds to the maximum value calculated among the three different cells.

A final comparison of the two scenarios of the SMO$||NMC_{622}$ cell chemistry ("baseline" and "optimistic") with the graphite$||NMC_{622}$ reference is presented in **Figure 10**. This comparison indicates that the reference cell chemistry remains superior to the alternative SMO-comprising cells with regard to the environmental impact, despite the slightly higher specific energy of the latter – at least at this early development stage and using the given synthesis method. Nonetheless, the "optimistic" scenario with an EUF of 0.5 and $Y = 95\%$ is approaching the reference cell chemistry in all impact categories apart from the 'resource depletion' – in this case the need for tin. In fact, this impact category might only be addressed by further increasing Y and/or by using recycled tin as the initial precursor; especially the latter appears to be a very powerful leverage to address this issue. The use of recycled materials and potentially different precursors might then also have an impact on the total energy demand, in addition to the scale-up, while the energy demand for the graphite production might be substantially underestimated, as discussed above. Consequently, it appears that the alternative SMO$||NMC_{622}$ cell chemistry might eventually (at least) compete with the graphite$||NMC_{622}$ reference when further optimizing the SMO synthesis.

3. Conclusions

A proof-of-concept large lab-scale prototype battery pack comprising $Sn_{0.9}Mn_{0.1}O_2$ (SMO), prepared by a continuous hydrothermal flow synthesis, as the active material for the negative electrode and commercial $LiNi_{0.6}Mn_{0.2}Co_{0.2}O_2$ (NMC_{622}) as active material for the positive electrode, was realized. Each pouch cell consisted of a double-side coated cathode and two single-side coated anodes. Three of these cells were connected in parallel forming one stack of cells and three of these stacks were connected in series to yield a voltage and current sufficiently high to power a remote-controlled electric vehicle for several hours. This alternative battery chemistry was moreover evaluated by an early-stage LCA and compared with the commercially well-established graphite$||NMC_{622}$ chemistry, serving as a reference. The results of this analysis show that the reference chemistry is presently favorable from the environmental point of view. However, the anticipated optimization of the SMO synthesis concerning energy use factor (EUF) and production (yield) in combination with the use of recycled tin instead of primary resources might eventually render the two cell chemistries competitive, while the specific energy and rate capability of the alternative is potentially (slightly) higher. This is particularly true when elevating the cut-off voltage upon charge and taking into account that recent attempts to reduce the uncertainty associated with the production of battery-grade graphite, as used in commercial LIBs, have revealed that its environmental footprint has been largely underestimated.

Additionally, these results nicely underline another important aim of this study: to motivate other scientists and researchers as well to go more often beyond the commonly used coin cells and to perform a continuous critical analysis of new alternative active (and inactive) materials in order to get an idea of the potential impact already at a rather early stage of development (despite the accordingly higher degree of uncertainty) and to identify remaining issues that need to be overcome prior to any potential application or scale-up of the battery cell fabrication.

4. Experimental Section

Synthesis of $Sn_{0.9}Mn_{0.1}O_2$: The synthesis of $Sn_{0.9}Mn_{0.1}O_2$ (SMO) used as the active material for the negative electrode had been reported in detail earlier[32] using an easily scalable hydrothermal synthesis.[54]

A schematic of the synthesis process is provided in Figure 4. Briefly, manganese(II) nitrate tetrahydrate (98%, Sigma–Aldrich) and potassium stannate (K_2SnO_3) trihydrate (99%, Sigma–Aldrich) were separately dissolved in deionized water. The two solutions were inserted into a continuous hydrothermal flow reactor [54,55] in stoichiometric amounts and mixed in a T-shaped mixing device. Additionally, supercritical (450 °C, 24.1 MPa) deionized water was delivered to meet the other combined solutions in a jet mixer, in which the nanoparticles were formed instantaneously. The resulting slurry was cooled down (pipe in pipe mixer) and brought to normal pressure after exiting the back pressure regulator. Subsequently, the water was removed from the product slurry and the wet solids were washed several times with deionized water, cleaned via dialysis, and finally freeze-dried. A comprehensive physicochemical characterization of the thus synthesized SMO nanoparticles was reported in Birrozzi et al.[32] A brief characterization by means of X-ray diffraction and high-resolution transmission electron microscopy was conducted using a Bruker D8 Advance (Cu-Kα radiation, $\lambda = 0.154$ nm) and an image Cs-corrected FEI Titan 80–300 kV at 300 kV, respectively.

Electrodes Preparation and Cell Assembly: Electrodes were prepared by dispersing the SMO active material and the conductive carbon (SuperC65, TIMCAL) in an aqueous solution of sodium carboxymethyl cellulose (CMC, Dow Wolff Cellulosics) in deionized water using a planetary ball mill (Fritsch Pulverisette 4). The weight ratio of the active material, conductive carbon, and binder was 75:20:5. The resulting electrode slurry was cast on dendritic copper foil (Schlenk, 99.9%) with a wet-film thickness of 120 µm. The wet electrodes were dried at room temperature overnight, cut into squared electrodes of 4.4×4.4 cm^2, and dried once more under vacuum at 120 °C for 24 h. The average active material mass loading was 2.5–3.0 mg cm^{-2}. The positive electrodes with NMC_{622} as active material were acquired from CUSTOMCELLS with an areal capacity of 3.5 mAh cm^{-2}. Squared electrodes of 4.0×4.0 cm^2 were cut in order to ensure a complete overlap of the positive electrodes with the negative electrodes. Consequently, the N:P ratio was ≈1.5 or 1.3 cm^{-2} (taking into account the first lithiation capacity of the negative electrode). As a separator a layer of Celgard 2325 was used, which was soaked with 800 µL of a 1M solution of $LiPF_6$ in a 1:1 mixture of ethylene carbonate (EC) and dimethyl carbonate (DMC), supplied by UBE. The pouch cells were assembled in the dry room with a dew point of less than –70 °C. Each pouch cell comprised a double-side coated positive electrode, sandwiched by two single-side coated negative electrodes in order to increase the capacity and, thus, energy per cell. The eventually prepared pack of pouch cells was used to power a remote-controlled vehicle (Top Gear Rally Car, LEGO). For the small-scale lithium-ion cell used to determine the average discharge voltage, the authors cut small discs with a diameter of 12 mm from both the SMO and the NMC_{622} electrode, and removed the electrode coating from one side of the double-side coated NMC_{622} electrode. Swagelok-type three-electrode cells were assembled in an argon-filled glove box with an oxygen and water content of less than 0.1 ppm. Metallic lithium foil (battery grade, Honjo) served as a reference electrode. The other cell components (electrolyte and separator) were the same as for the large pouch cells.

Electrochemical Characterization: For the galvanostatic cycling of the three-electrode cell, a multi-channel potentiostat/galvanostat (BioLogic. VMP-3) was used. The cut-off voltages were set to 0.01 V and 3.0 V for the negative electrode and to 2.5 and 4.1 V for the positive electrode. The specific current applied was 5 mA g^{-1}.

To estimate the current needed to power the remote-controlled vehicle, a single-channel potentiostat (BioLogic, VMP-200) was utilized and the voltage applied was set to 9.0 V. The lab-scale prototype cells were charged by means of a Maccor battery tester, setting the upper cut-off voltage to 4.1 V and applying a current of 11 mA. The prototype battery pack was charged in three parts, i.e., always three cells connected in parallel in order to not exceed the voltage limit of the channel. The temperature for the two galvanostatic experiments was 20 °C, while the constant voltage experiment was conducted at room temperature.

Life Cycle Assessment – Methodology: The life cycle assessment of the active materials in the electrodes for the scaled-up cell was performed in accordance with the guidelines established in the ISO standards 14040/14044 for the LCA methodology.[56] The life cycle stages considered in the analysis were those comprised in the cradle-to-gate approach, which describes the mass and energy flows along the initial life cycle stages of the system and until the gate of the factory where it is produced. These stages are mainly associated with resource extraction, supply chain, and system manufacture. The use-phase and end-of-life were excluded from the analysis, as these stages entail a high degree of uncertainty for an emerging technology. The environmental impacts of the system were described in terms of a functional unit which, for the specific case, was defined as 1 Wh of cell capacity. Generally, the LCA methodology offers a broad range of impact assessment methods (LCIA), each comprising a predefined set of impact categories focusing on specific areas of concern. These categories encompass the environmental implications of using potentially scarce natural resources and various potential emissions into the biosphere such as greenhouse gases, acidification agents, and particulates with an impact on human health.

Each category is described in units of equivalence used to quantify the corresponding impacts as a function of a reference compound or resource. All the material and energy flow coming in and out of the system (i.e., from and to the biosphere) are translated into the respective units via characterization factors allocated to each flow. According to the recommendations of the product environmental footprint category rules for rechargeable batteries by the European Commission,[57] the most relevant impact categories for the study of battery systems are "acidification" (terrestrial and freshwater), "climate change", "resource depletion" (energy carriers and minerals) and respiratory inorganics (herein referred to as "particulate matter"). In this case, the chosen LCIA is the ILCD 2011 Midpoint+ provided in the LCIA method package 2.1.1 by the consultancy and software development company Green Delta (https://nexus.openlca.org/) and implemented in the software OpenLCA. The impact categories of interest can be found within the ILCD Midpoint methodology labeled in the following manner: "acidification", indicating the potential damage to soil and waters from the release of acidifying agents and measured in molc (moles of charge) H^+ eq; "climate change", related to the emission of CO_2 and other greenhouse gases measured in kg CO_2 eq; "mineral, fossil, and renewable resource depletion" (kg Sb eq), herein referred to as "resource depletion" and related to the extraction of abiotic resources; and "particulate matter" (kg PM2.5 eq), covering the effects of fine particulates with an aerodynamic diameter of less than 2.5 µm.[58] An estimation of the CED, expressed in MJ/MWh is also offered as a reference for the energy intensity. The analysis performed herein largely focuses on the findings for the negative electrode, as the positive electrode was the same for the two cell chemistries and since there are many studies reported for conventional LIBs.[39,59–78] For the sake of completeness, however, the full list of all sixteen categories of the ILCD method are presented in Table S2, Supporting Information.

Owing to the premature state of the technical development of the anode active material synthesis, a sensitivity analysis was performed to assess the uncertainty of the results in the face of changing conditions. The sensitivity of the SMO production to material yield and energy demand was estimated separately and for a certain range of values. These parameters were selected based on their suitability to reflect changing process efficiencies, typically resulting from scaled-up manufacturing. Eventually, a comparison with a conventional graphite‖NCM_{622} cell was conducted as a benchmark for the potential of the novel system.

Life Cycle Assessment – System Modelling: The first stage of the analysis assessed the potential environmental performance of the SMO active material. This assessment took into account the performance of the anode material (SMO vs graphite) in combination with the cathode active material NMC_{622}. To compare the specific energy of the two battery chemistries SMO‖NMC_{622} and graphite‖NMC_{622}, the experimentally obtained specific capacities and delithiation profiles of a commercial graphite anode (SLP30, IMERYS) and an SMO anode in half-cell

configuration were used, providing 363 and 612 mAh g^{-1}, respectively, up to an upper cut-off of 1.0 V. For the NMC_{622} cathode we assumed an average lithiation potential of 4.0 V vs. Li^+/Li and a theoretical capacity of 160 mAh g^{-1}. The N:P ratio was set to 1.1. The results are summarized in Table S1, Supporting Information. A calculation of the specific energy for a graphite‖NMC_{622} cell using the BatPaC tool developed by the Argonne National Laboratory in the USA yields a specific energy of 231 Wh kg^{-1} at the cell level for the graphite‖NMC_{622} cell chemistry, i.e., approximately half of the value calculated for the active material level. Assuming a comparable cell composition, the same ratio was used for the estimation of the specific energy of the SMO‖NMC_{622} at the cell level, yielding 237 Wh kg^{-1}, i.e., a slight increase. The cell composition used for the LCA, as summarized in Table S3, Supporting Information, followed a previous study by Peters and Weil[61] and takes into account the different anode/cathode active material ratio for the two different cell chemistries (assuming an N:P ratio of 1.1).

The life cycle inventories (LCI), i.e., datasets describing the mass and energy flows of the assessed products, were constructed by implementing a hybrid approach that incorporated data from different sources and for products at different technology readiness levels. This procedure was chosen owing to the early stage of development of SMO, which was synthesized using a pilot line, so there was no data available for a fully developed synthesis at the industrial level. Two scenarios were considered: i) A baseline scenario, taking into account the pilot line data, and ii) an optimistic scenario, emulating an increased efficiency of the SMO synthesis to enable a fairer comparison with the well-developed graphite reference system. Further details of the two different scenarios are provided along with the discussion of the results. The production of the main SMO precursors such as potassium stannate trihydrate and manganese nitrate tetrahydrate were modeled based on the synthesis methods reported in the literature.[79,80] The average European ENTSO-E electricity mix as found in Ecoinvent was used for the modeling of the production of the anode material. More details concerning the inventories are provided in Table S5–S10, Supporting Information.

The LCA of the full-cells follows a model earlier reported by Peters and Weil,[69] who developed a unified LCI for a conventional graphite‖NCM_{622} cell based on the most frequently used inventories reported in the literature. The data for the supply chain, transportation, infrastructure, and other processes associated with the cell manufacturing were extracted from the commercial database Ecoinvent V3.7.1.

Supporting Information

Supporting Information is available from the Wiley Online Library or from the author.

Acknowledgements

A.B. S.P.B. contributed equally to this work. Financial support from the Vector Foundation within the NEW E^2 project and the Helmholtz Association is kindly acknowledged (A.B., T.E., J.A., G.-T.K., and D.B.). UCL (J.A.D., A.R.G., C.S., and T.E.A.) acknowledges the support of EPSRC JUICED Energy hub project EP/R023662/1.

Open access funding enabled and organized by Projekt DEAL.

Conflict of Interest

The authors declare no conflict of interest.

Data Availability Statement

The data that support the findings of this study are available from the corresponding author upon reasonable request.

Keywords

battery pack, doping, electric vehicle, LCA, lithium-ion battery, NMC_{622}, SnO_2

Received: March 4, 2022
Revised: July 1, 2022
Published online:

[1] D. Bresser, A. Moretti, A. Varzi, S. Passerini, in *Encyclopedia of Electrochemistry*, (Ed.: A. J. Bard), Wiley, New York **2020**, pp. 1–9.
[2] M. Armand, P. Axmann, D. Bresser, M. Copley, K. Edström, C. Ekberg, D. Guyomard, B. Lestriez, P. Novák, M. Petranikova, W. Porcher, S. Trabesinger, M. Wohlfahrt-Mehrens, H. Zhang, *J. Power Sources* **2020**, *479*, 228708.
[3] M. Marinaro, D. Bresser, E. Beyer, P. Faguy, K. Hosoi, H. Li, J. Sakovica, K. Amine, M. Wohlfahrt-Mehrens, S. Passerini, *J. Power Sources* **2020**, *459*, 228073.
[4] H. C. Hesse, M. Schimpe, D. Kucevic, A. Jossen, *Energies* **2017**, *10*, 2107.
[5] H. Rallo, L. Canals Casals, D. De La Torre, R. Reinhardt, C. Marchante, B. Amante, *J. Clean. Prod.* **2020**, *272*, 122584.
[6] D. T. Wrublewski, *Sci. Technol. Librar.* **2020**, *39*, 51.
[7] P. V. Kamat, *ACS Energy Lett.*. **2019**, *4*, 2757.
[8] Y. Nishi, *Chem. Rec.* **2001**, *1*, 406.
[9] J. Asenbauer, T. Eisenmann, M. Kuenzel, A. Kazzazi, Z. Chen, D. Bresser, *Sustainable Energy Fuels* **2020**, *4*, 5387.
[10] J. Wolfenstine, J. L. Allen, J. Read, D. Foster, *Chemistry and Structure of Sony's Nexelion Li-Ion Electrode Materials*, Defense Technical Information Center, Ft. Belvoir **2006**.
[11] Z. Lin, X. Lan, X. Xiong, R. Hu, *Mater. Chem. Front.* **2021**, *5*, 1185.
[12] B. N. Loeffler, D. Bresser, S. Passerini, M. Copley, *Johnson Matthey Technol. Rev.* **2015**, *59*, 34.
[13] M. N. Obrovac, V. L. Chevrier, *Chem. Rev.* **2014**, *114*, 11444.
[14] N. Nitta, G. Yushin, *Part. Part. Syst. Charact.* **2014**, *31*, 317.
[15] X. Wu, Y. Bai, Z. Li, J. Liu, K. Zhao, Z. Du, *J. Energy Chem.* **2021**, *56*, 121.
[16] S. Chen, K. Wen, J. Fan, Y. Bando, D. Golberg, *J. Mater. Chem. A* **2018**, *6*, 11631.
[17] T. Tsujikawa, K. Yabuta, M. Arakawa, K. Hayashi, *J. Power Sources* **2013**, *244*, 11.
[18] S. Fang, D. Bresser, S. Passerini, *Adv. Energy Mater.* **2020**, *10*, 1902485.
[19] D. Bresser, S. Passerini, B. Scrosati, *Energy Environ. Sci.* **2016**, *9*, 3348.
[20] W. Ni, J. Cheng, L. Shi, X. Li, B. Wang, Q. Guan, L. Huang, G. Gu, H. Li, *J. Mater. Chem. A* **2014**, *2*, 19122.
[21] Z. Wei, L. Wang, M. Zhuo, W. Ni, H. Wang, J. Ma, *J. Mater. Chem. A* **2018**, *6*, 12185.
[22] D. Bresser, F. Mueller, M. Fiedler, S. Krueger, R. Kloepsch, D. Baither, M. Winter, E. Paillard, S. Passerini, *Chem. Mater.* **2013**, *25*, 4977.
[23] F. Mueller, D. Geiger, U. Kaiser, S. Passerini, D. Bresser, *ChemElectroChem* **2016**, *3*, 1311.
[24] A. Trapananti, T. Eisenmann, G. Giuli, F. Mueller, A. Moretti, S. Passerini, D. Bresser, *Mater. Today Chem.* **2021**, *20*, 100478.
[25] J. Asenbauer, J. R. Binder, F. Mueller, M. Kuenzel, D. Geiger, U. Kaiser, S. Passerini, D. Bresser, *ChemSusChem* **2020**, *13*, 3504.
[26] F. Mueller, D. Bresser, V. S. K. Chakravadhanula, S. Passerini, *J. Power Sources* **2015**, *299*, 398.
[27] T. Eisenmann, A. Birrozzi, A. Mullaliu, J. Asenbauer, G. Giuli, A. Trapananti, L. Olivi, H. Moon, D. Geiger, U. Kaiser, S. Passerini, D. Bresser, *J. Phys. Chem. C* **2021**, *125*, 8947.
[28] J. Wu, N. Luo, S. Huang, W. Yang, M. Wei, *J. Mater. Chem. A* **2019**, *7*, 4574.

[29] J. Asenbauer, M. Kuenzel, T. Eisenmann, A. Birrozzi, J.-K. Chang, S. Passerini, D. Bresser, *J. Phys. Chem. Lett.* **2020**, *11*, 8238.
[30] Y. Ma, Y. Ma, U. Ulissi, Y. Ji, C. Streb, D. Bresser, S. Passerini, *Electrochim. Acta* **2018**, *277*, 100.
[31] T. Eisenmann, A. Birrozzi, A. Mullaliu, G. Giuli, A. Trapananti, S. Passerini, D. Bresser, *J. Electrochem. Soc.* **2021**, *168*, 030503.
[32] A. Birrozzi, J. Asenbauer, T. E. Ashton, A. R. Groves, D. Geiger, U. Kaiser, J. A. Darr, D. Bresser, *Batteries Supercaps* **2020**, *3*, 284.
[33] N. Wan, X. Lu, Y. Wang, W. Zhang, Y. Bai, Y.-S. Hu, S. Dai, *Sci. Rep.* **2016**, *6*, 18978.
[34] Y. Ma, Y. Ma, G. Giuli, T. Diemant, R. J. Behm, D. Geiger, U. Kaiser, U. Ulissi, S. Passerini, D. Bresser, *Sustainable Energy Fuels* **2018**, *2*, 2601.
[35] M.-S. Balogun, W. Qiu, Y. Luo, H. Meng, W. Mai, A. Onasanya, T. K. Olaniyi, Y. Tong, *Nano Res.*. **2016**, *9*, 2823.
[36] F. De Giorgio, N. Laszczynski, J. von Zamory, M. Mastragostino, C. Arbizzani, S. Passerini, *ChemSusChem* **2017**, *10*, 379.
[37] M. Messagie, L. Oliveira, S. Rangaraju, J. S. Forner, M. H. Rivas, in *Rechargeable Lithium Batteries*, (Ed.: A. A. Franco), Woodhead Publishing, Sawston, United Kingdom **2015**, pp. 303–318.
[38] M. Raugei, P. Winfield, *J. Cleaner Prod.* **2019**, *213*, 926.
[39] M. Mohr, J. F. Peters, M. Baumann, M. Weil, *J. Ind. Ecol.* **2020**, *24*, 1310.
[40] M. Pagliaro, F. Meneguzzo, *Heliyon* **2019**, *5*, e01866.
[41] H.-J. Liang, Z.-Y. Gu, X.-X. Zhao, J.-Z. Guo, J.-L. Yang, W.-H. Li, B. Li, Z.-M. Liu, W.-L. Li, X.-L. Wu, *Angew. Chem., Int. Ed.* **2021**, *60*, 26837.
[42] L. Zhang, H. Dong, H. Wei, E. H. Ang, J. Yang, X. Miao, H. Geng, X. Zuo, *J. Power Sources* **2021**, *506*, 230216.
[43] X. Rui, X. Zhang, S. Xu, H. Tan, Y. Jiang, L. Y. Gan, Y. Feng, C. C. Li, Y. Yu, *Adv. Funct. Mater.* **2021**, *31*, 2009458.
[44] L. Xie, H. Liu, S. Lin, X. Yang, M. Qi, L. Zhu, Y. Guo, G. Guo, *RSC Adv.* **2019**, *9*, 11369.
[45] J. Lopez, D. G. Mackanic, Y. Cui, Z. Bao, *Nat. Rev. Mater.* **2019**, *4*, 312.
[46] F. Wang, B. Wang, J. Li, B. Wang, Y. Zhou, D. Wang, H. Liu, S. Dou, *ACS Nano* **2021**, *15*, 2197.
[47] R. Zhan, X. Wang, Z. Chen, Z. W. Seh, L. Wang, Y. Sun, *Adv. Energy Mater.* **2021**, *11*, 2101565.
[48] H. Zhang, L. Wang, H. Li, X. He, *ACS Energy Lett.*. **2021**, *6*, 3719.
[49] L. Liang, X. Sun, C. Wu, L. Hou, J. Sun, X. Zhang, C. Yuan, *ACS Appl. Mater. Interfaces* **2018**, *10*, 5498.
[50] T. Lei, Z. Yang, Z. Lin, X. Zhang, *Chin. J. Aeronaut.* **2019**, *32*, 1488.
[51] A. Birrozzi, A. Mullaliu, T. Eisenmann, J. Asenbauer, T. Diemant, D. Geiger, U. Kaiser, D. Oliveira de Souza, T. E. Ashton, A. R. Groves, J. A. Darr, S. Passerini, D. Bresser, *Inorganics* **2022**, *10*, 46.
[52] E. A. Olivetti, G. Ceder, G. G. Gaustad, X. Fu, *Joule* **2017**, *1*, 229.
[53] P. Engels, F. Cerdas, T. Dettmer, C. Frey, J. Hentschel, C. Herrmann, T. Mirfabrikikar, M. Schueler, *J. Cleaner Prod.* **2022**, *336*, 130474.
[54] J. A. Darr, J. Zhang, N. M. Makwana, X. Weng, *Chem. Rev.* **2017**, *117*, 11125.
[55] Jawwad Darr, *Co-Current Mixer Apparatus, Reactor and Method for Precipitating Nanoparticles*, **2015**, US 9,192,901 B2.
[56] ISO INTERNATIONAL STANDARD. Environmental management Life cycle assessment Principles and framework – PDF Free Download, https://docplayer.net/2540011-Iso-14040-international-standard-environmental-management-life-cycle-assessment-principles-and-framework.html (accessed: April 2022).
[57] PEFCR - Product Environmental Footprint Category Rules for High Specific Energy Rechargeable Batteries for Mobile Applications, **2018**.
[58] European Commission, Joint Research Centre, Institute for Environment and Sustainability, *International Reference Life Cycle Data System (ILCD) Handbook General Guide for Life Cycle Assessment: Provisions and Action Steps*, Publications Office, Luxembourg **2011**.
[59] A. Accardo, G. Dotelli, M. L. Musa, E. Spessa, *Appl. Sci.* **2021**, *11*, 1160.
[60] M. A Cusenza, S. Bobba, F. Ardente, M. Cellura, F. Di Persio, *J. Clean. Prod.* **2019**, *215*, 634.
[61] L. da Silva Lima, M. Quartier, A. Buchmayr, D. Sanjuan-Delmás, H. Laget, D. Corbisier, J. Mertens, J. Dewulf, *Sustainable Energy Technol. Assess.* **2021**, *46*, 101286.
[62] Q. Dai, J. C. Kelly, L. Gaines, M. Wang, *Batteries* **2019**, *5*, 48.
[63] L. A.-W. Ellingsen, G. Majeau-Bettez, B. Singh, A. K. Srivastava, L. O. Valøen, A. H. Strømman, *J. Ind. Ecol.* **2014**, *18*, 113.
[64] E. Kallitsis, A. Korre, G. Kelsall, M. Kupfersberger, Z. Nie, *J. Cleaner Prod.* **2020**, *254*, 120067.
[65] J. C. Kelly, Q. Dai, M. Wang, *Mitig. Adapt. Strateg. Glob. Change* **2020**, *25*, 371.
[66] H. C. Kim, T. J. Wallington, R. Arsenault, C. Bae, S. Ahn, J. Lee, *Environ. Sci. Technol.* **2016**, *50*, 7715.
[67] T. Le Varlet, O. Schmidt, A. Gambhir, S. Few, I. Staffell, *J. Energy Storage* **2020**, *28*, 101230.
[68] Y. Liang, J. Su, B. Xi, Y. Yu, D. Ji, Y. Sun, C. Cui, J. Zhu, *Resour., Conserv. Recycl.* **2017**, *117*, 285.
[69] G. Majeau-Bettez, T. R. Hawkins, A. H. Strømman, *Environ. Sci. Technol.* **2011**, *45*, 4548.
[70] P. Marques, R. Garcia, L. Kulay, F. Freire, *J. Cleaner Prod.* **2019**, *229*, 787.
[71] D. A. Notter, M. Gauch, R. Widmer, P. Wäger, A. Stamp, R. Zah, H.-J. Althaus, *Environ. Sci. Technol.* **2010**, *44*, 6550.
[72] J. F. Peters, M. Baumann, B. Zimmermann, J. Braun, M. Weil, *Renewable Sustainable Energy Rev.* **2017**, *67*, 491.
[73] J. F. Peters, M. Weil, *J. Cleaner Prod.* **2018**, *171*, 704.
[74] X. Shu, Y. Guo, W. Yang, K. Wei, G. Zhu, *Energy Rep.* **2021**, *7*, 2302.
[75] X. Sun, X. Luo, Z. Zhang, F. Meng, J. Yang, *J. Cleaner Prod.* **2020**, *273*, 123006.
[76] S. Wang, J. Yu, *Waste Manag. Res.* **2021**, *39*, 156.
[77] Z. Wu, D. Kong, *Clean Technol. Environ. Policy* **2018**, *20*, 1233.
[78] M. Zackrisson, L. Avellán, J. Orlenius, *J. Cleaner Prod.* **2010**, *18*, 1519.
[79] R. E. Horn, *Production of Potassium or Sodium Stannate*, **1978**, US4066518A.
[80] J. Y. Welsh, A. Mullier, P. C. Picquet, *Process for Preparing Manganese Nitrate Solution*, **1985**, EP0065608B1.